Journal of Fluids and Structures 17 (2003) 717–738

JOURNAL OF FLUIDS AND STRUCTURES

www.elsevier.nl/locate/jnlabr/yjfls

Three-dimensionality development inside standard parallelepipedic lid-driven cavities at Re = 1000

C. Migeon[a,*], G. Pineau[b], A. Texier[b]

[a] *Laboratoire de Mécanique Appliquée, Automatique et Géomécanique (LMA2G), Institut National des Sciences Appliquées (INSA) 20 avenue des Buttes de Coësmes-CS 14315, 35043 Rennes cedex, France*

[b] *Laboratoire d'Etudes Aérodynamiques (LEA), Université de Poitiers, UMR/CNRS 6609, Boulevard Marie et Pierre CURIE Téléport 2, BP 179, 86960 Futuroscope cedex, France*

Received 20 November 2000; accepted 12 December 2002

Abstract

This paper considers the problem of the time-dependent laminar incompressible flow motion within parallelepipedic cavities in which one wall moves with uniform velocity after an impulsive start using a particle-streak and a dye-emission techniques. Of particular concern is the examination of the spanwise structures of the flow in view to point out how three-dimensionality arises and develops with time for a Reynolds number of 1000. For this purpose, attention is focused on the spanwise currents, the end-wall corner vortices and the structures resulting from the centrifugal instability. Among others, the study clearly shows the scenario of propagation of the spanwise currents by giving quantitative information on their velocity and on the time from which a given cross-plane becomes affected by such a 3-D perturbation. Furthermore, the numerous visualizations reveal the existence of only one corner-vortex on each end-wall; this vortex is quasi-toroidal shaped. Finally, concerning flow instability, the present results show that no well-formed counter-rotating vortices emerge for Re = 1000 during the start-up phase contrary to what was asserted so far. However, two successive initial phases of this instability development are revealed for the first time.

1. Introduction

1.1. Lid-driven cavity flows

Viscous rotating flows are the base of a large variety of natural, industrial and biomedical applications. Among them, lid-driven cavity flows (in which the contained fluid is set into motion by a translating lid) are of primary importance and are regularly the object of researches. Indeed, this type of flows is, without any doubt, one of the simplest examples to study both physical and fundamental characteristics of recirculating flows. Furthermore, it is in direct relevance to many practical applications ranged from purely engineering ones to medical ones (Savvides and Gerrard, 1984; Aidun et al., 1991; Gaskell et al., 1996; Liou and Liao, 1997).

However, despite their apparent simple geometry, lid-driven cavity flows are known to contain high degrees of complexity revealing 3-D flow structures even at large spanwise aspect ratio (SAR). Thus, since the pioneer numerical work of De Dahl Davis and Mallinson (1976), literature abounds in experimental and numerical studies related to the three-dimensionality of lid-driven cavity flows with emphasis on analyzing the fully established regime of the square-

*Corresponding author. Dept Génie Agronomique, Institut National d'Horticulture, Unité Mixte de Recherche SAGAH, 2 rue le Nôtre, 49045 Angers cedex 01, France.

E-mail address: christophe.migeon@inh.fr (C. Migeon).

0889-9746/03/$ - see front matter
doi:10.1016/S0889-9746(03)00009-4

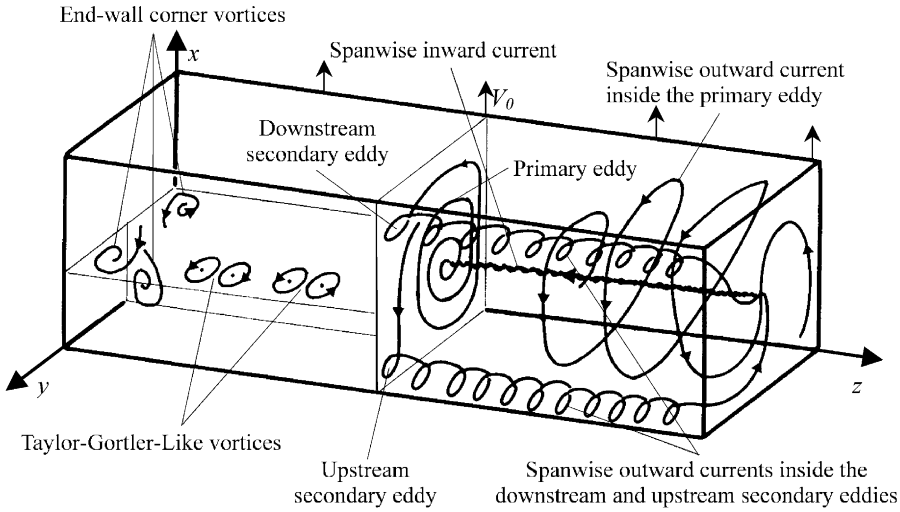

Fig. 1. Structure of the fully developed flow in the square cavity.

section cavity (Koseff and Street, 1982, 1984a–c; Freitas and Street, 1988; Freitas et al., 1985; Ghia et al., 1982). A recent comprehensive literature review gives extensive accounts of their works (Shankar and Deshpande, 2000).

It is pointed out that for Reynolds numbers in the range $1500 \leqslant Re \leqslant 10000$, the square-section cross-sectional flow (plane parallel to oxy; Fig. 1) is basically characterized by a large primary eddy and three secondary eddies located near the cavity corners. These secondary eddies are usually referred to as the downstream secondary eddy, the upstream secondary eddy and the lower secondary eddy. In spanwise views, for the fully developed regime, both experimental and numerical studies have shown the presence of three main 3-D structures: the spanwise inward and outward currents, the end-wall corner vortices and the Taylor–Gortler-like (TGL) counter-rotating vortices (only if the SAR is greater than or equal to 0.5; Prasad et al., 1988); all three are represented in Fig. 1. The spanwise currents and the corner vortices are directly induced by the no-slip conditions imposed at end-walls; they are hereafter named the primary 3-D structures. With regard to the TGL vortices, most of the researchers contended that they develop on account of a centrifugal instability induced by the concave-separated streamline between the primary eddy and the downstream secondary eddy (similarly to the Taylor vortices occurring between rotating cylinders and the Gortler ones occurring in the boundary layer over a concave surface). These vortex pairs are dispersed along the cavity span and can meander in the spanwise direction if SAR is greater than or equal to 1:1 (also, their number greatly depends on Reynolds number and SAR).

According to the Stanford's researchers (Koseff and Street, 1982, 1984a–c), the TGL vortices are issued from transient toroidal vortices [named Taylor-like (TL) vortices] which develop during the start-up flow phase for $1000 \leqslant Re \leqslant 10000$ (study performed for SAR of 3:1). However, even if TL and TGL vortices represent the same flow structure, authors insist on their distinction because, in their opinion, those specific vortices originate from two different kinds of instability.

For the numerical studies, the 3:1 square-cavity at $Re = 3200$ has been selected as a benchmark configuration. In spite of general agreements between results, quite different conclusions arise especially concerning flow symmetry, number and localization of TGL vortices (Deville and Morchoisne, 1992). These disagreements are particularly due to the complexity of the 3-D dynamics of the flow which translated in the difficulty of accurately reproducing fine spatial and temporal features. Moreover, at the present time, the TL vortices have not been simulated yet.

Taking into account these discrepancies, in the past recent years, some researchers considered Reynolds numbers lower than 3200 in order to accurately understand the 3-D cavity flow dynamics. In such a context, at the end of the 1990s, Chiang et al. (1997, 1998) and Chiang and Sheu (1997) initiated a series of numerical works devoted to the 3:1 square-section cavity at Reynolds numbers close to 1000. They also found that the development of TGL vortices is due to a centrifugal instability but they show that this instability develops near the concave separation-line of the upstream secondary eddy and not near the one of the downstream secondary eddy as previously proclaimed. It is noteworthy that the fact the separation line of the upstream secondary eddy also triggered instability has been first pointed out by Hou (1995) as mentioned in the recent paper of Teixeira (1997). Moreover, Chiang et al. showed that the Taylor–Gortler vortices appear for Reynolds number greater than or equal to 1300, whereas these vortices, and the initial Taylor ones, were observed as soon as $Re = 1000$ by the Stanford group's experiments for the same SAR of 3:1.

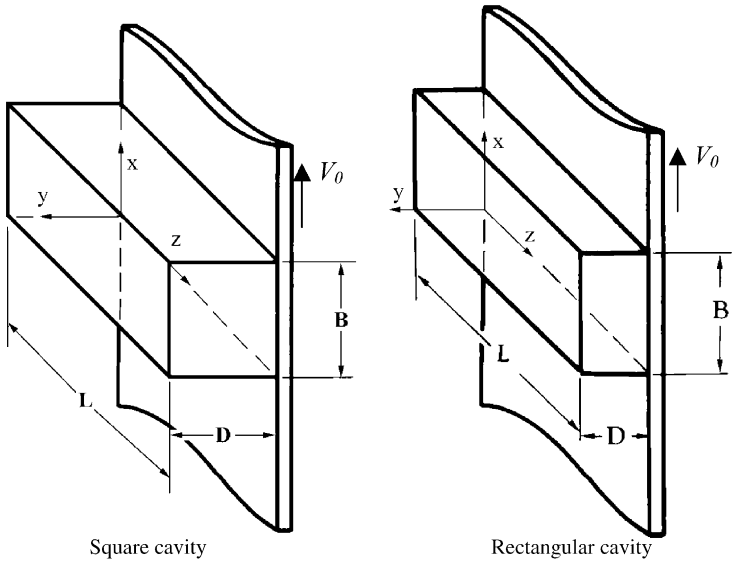

Fig. 2. Cavity nomenclature and reference frame.

1.2. Aim of the study

As a result of this short review, it appears that despite several decades of experiments and computations, the 3D incompressible LDC flows still raise open questions even at the moderate Reynolds number Re = 1000. Also, at the present time, it is not clear how three-dimensionalities arise and settle with time after the start of the motion; only a very fragmentary description of the start-up flow phase has been given by the Stanford experimental group. The main reason of this lack probably rests in the technical difficulties encountered to ensure experiments during the typical start-up phase.

The current experimental investigation focuses on the 3-D aspect of lid-driven cavity flows with a view to closely examine the way the three-dimensionalities develop with time from rest at Re = 1000. For this study, two rather short (SAR = 2:1) parallelepipedic cavities have been considered: a square-section one and a shallow rectangular-section one (Fig. 2). This experimental study is based upon a detailed analysis of flow visualizations performed with a particle-streak and a dye-emission techniques (see Section 2.2). Pictures have been taken in different cross planes but also spanwise to plainly appreciate the 3-D degeneration of the flow structure (spanwise pictures have been taken over the whole span of the cavity in order to clarify the ambiguity in the flow symmetry).

This work follows the Poitiers's group previous studies which have been so far interested in 3-D body-end effects in the wakes of various types of cylinders (Champion and Coutanceau, 1992; Pineau, 1992; Pineau et al., 1992; Polidori et al., 1992; Polidori, 1994; Coutanceau and Pineau, 1997) and even in the development of TGL vortices in the wake of a semicircular shell (Ehrmann, 1996; Coutanceau et al., 2000). In the midst of the 1990s, the Poitiers's group (France) initiated a series of experimental works devoted to the comprehension of the transient regime inside variously shaped lid-driven cavities (Coutanceau et al., 1996; Migeon et al., 1998, 2000; Guermond et al., 2002; Migeon, 2000).

In the following section a brief description of the experimental set-up and the visualization techniques is given. Then, the development of 3-D structures is described and their dependence on the cavity shape is examined. Finally, a conclusion is given.

2. Experimental apparatus and methods

2.1. Experimental apparatus

For the present study a specific and efficient experimental set-up, already used in wake-studies (Pineau et al., 1992; Ohmi et al., 1991; Badr et al., 1990), was used. This apparatus is schematized in Fig. 3 and finely described in a previous paper (Migeon et al., 2000). Thereby, the details of the experimental apparatus are not reported here, only a brief description of its main components is recalled.

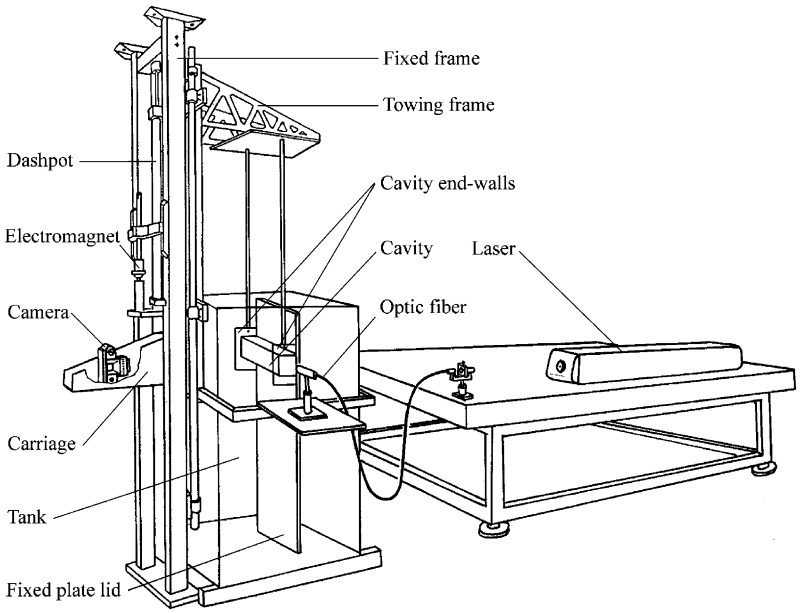

Fig. 3. Experimental apparatus.

The cavity, attached to a mobile carriage by metal rods, is immersed in a water tank ($Wt \times Lt \times Ht = 100 \times 100 \times 150\,cm^3$) and lies along a fixed vertical plate which acts as the cavity lid. The cavity is completely enclosed so that the fluid cannot escape.

After an impulsive start (the mobile carriage acceleration phase corresponds to a very short time period of about 0.05 s, i.e., 1.45% of the dimensionless time unit), the cavity translates vertically along its lid at a constant speed V_0 which has been selected for the present work to 1.8 cm/s; the cavity speed remains quasi-constant within a variation range of 1%. As usual, the Reynold number is based on the cavity height and the lid velocity ($Re = V_0 B/\nu$).

Flow pictures are recorded by a computer-controlled camera which follows the cavity downfall. Pictures are captured during a period of normalized time t^* ($t^* = tV_0/B$) ranging from 0 (start of the motion) to 12 (the limit imposed by the height of the tank) in steps $\Delta t^* = 1$. Thus, the last flow recording is made after the cavity has travelled a distance equal to $12B$. In such a configuration, the cavity appears to be at rest in the camera frame and submitted to the upward motion of the vertical plate (moving lid). In all the pictures presented in this paper, the relative uniform lid translation goes from base to top.

As mentioned above, two parallelepipedic cavities are examined (Fig. 2). Both cavities have a similar height B (6.2 cm) and length L (12.4 cm) thus defining a SAR of 2:1 (cavities are limited in span by stationary end-walls). For the rectangular cavity, $B = 2 * D$.

$0xyz$ is the cavity system coordinates, with the origin located at the lower right corner on the end-wall plane. Each measurement along the three axes is nondimensionalized by the cavity height B such that $X = x/B$, $Y = y/B$ and $Z = z/B$.

2.2. Visualization techniques

In order to appreciate the 3-D flow structure, and according to the type of information required, two complementary visualization techniques are used: the continuous dye-emission one and the particle-streak one.

The dye-emission technique is based on a continuous electrolytic process of nine tin-ribbons (anode). The latter are uniformly spaced out along the cavity span and set in grooves tooled in the downstream wall of the cavity (detail A, Fig. 4). The cathode is a copper sheet immersed in the tank. The white "dye" produced by the tin electrolyze is convected into the cavity area by the flow movement thus giving information on mass transport and on mixing process. In order to visualize the dye propagation, the cavity is lit by a volumic white light or by a thin laser sheet, whether the span fluid-movement or the cross-plane one is observed. Note that considerable technical skill is needed to finely machine the ribbon grooves and to precisely polish the cavity wall surface in order to avoid wall perturbations which might increase the unstable character of the flow (Migeon, 2000; Guermond et al., 2002).

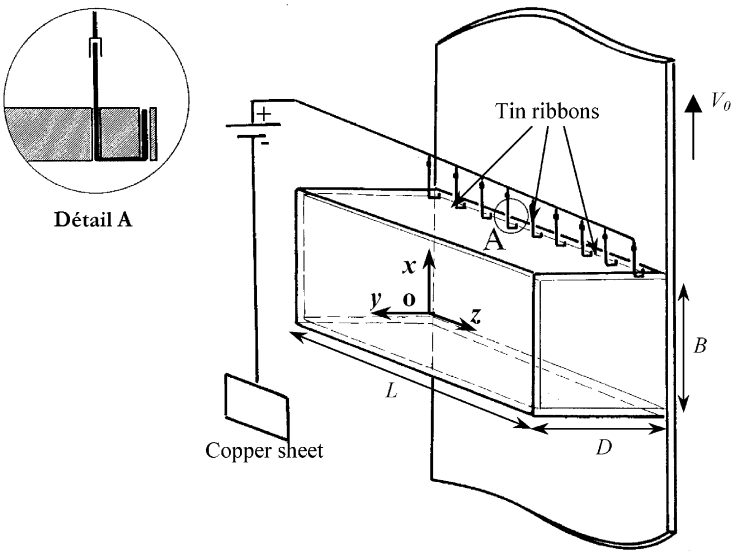

Fig. 4. Principle of the dye-emission technique.

The particle-streak technique involves seeding tiny particles in the cavity area. Planes are illuminated by a thin laser sheet of about 2 mm in thickness. During the time exposure, particles describe their paths giving access to instantaneous streak fields which provide information on both flow topology and kinematics if this time of exposure is sufficiently short (see Pineau et al., 1992; Ohmi et al., 1991; Badr et al., 1990; Coutanceau and Pineau, 1997, where particle-streak visualizations are compared with numerical pictures). Because of the flow complexity, flow patterns have been visualized in various horizontal and vertical span-planes. For both cavities, the horizontal planes are $X = 0.25$, 0.5 and 0.75. The vertical planes are $Y = 0.125$, 0.25, 0.3125, 0.375, 0.5, 0.75, 0.875 for the square cavity, and $Y = 0.125$, 0.25, 0.375, 0.4375 for the rectangular cavity.

3. Dye-filament visualizations: analysis of the spanwise current establishment

3.1. Qualitative examination

In a first step, the time-evolution of the global three-dimensionality of the flow is considered by examining the development of the spanwise currents. The existence of these spanwise currents coming from the cavity end-extremities and the way they propagate with time into the primary eddy core are shown in Figs. 5 and 6, respectively, for the square and rectangular cavities. On each sequence, the volumic spanwise view of the flow is compared to the symmetry-plane view ($Z = 1$).

In cross-planes, the dye-filament penetrates the cavity in the form of a rolling-up filament depicting the mixing process inside the primary eddy (see Migeon et al., 2000 for quantitative comparisons of the mixing-zone area between the square and the rectangular cavities). In the square cavity, the filament develops regularly, keeping a quite rounded shape. In contrast, in the rectangular cavity, the filament elongates in the opposite direction of the lid motion due to the combined effects of the cavity bottom-wall (left-wall) and of the development of the large upstream secondary eddy which flattens the main recirculation zone.

At $t^* = 1$, each filament rolls-up inside its own section of emission indicating that the initial flow (along most of the span) can be assimilated to a 2-D flow with a good approximation (see Migeon, 2000 for quantitative data). However, one can note that, at each end-walls, the end filaments begin to develop axially towards the symmetry plane indicating the onset of the flow three-dimensionality (Figs. 5 and 6). These two opposite currents result from the interaction between the primary eddy and the viscous damping effects on the end-walls: a negative spanwise pressure gradient is induced from the end-walls towards the symmetry plane (Chiang et al., 1997). Later on ($t^* > 2$), the dye filaments continue to progress towards the symmetry plane, successively crossing all the emitting sections up to the symmetry plane. This implies the initial 2-D roll-up of each filament to develop in the spanwise direction in a spiral form having a

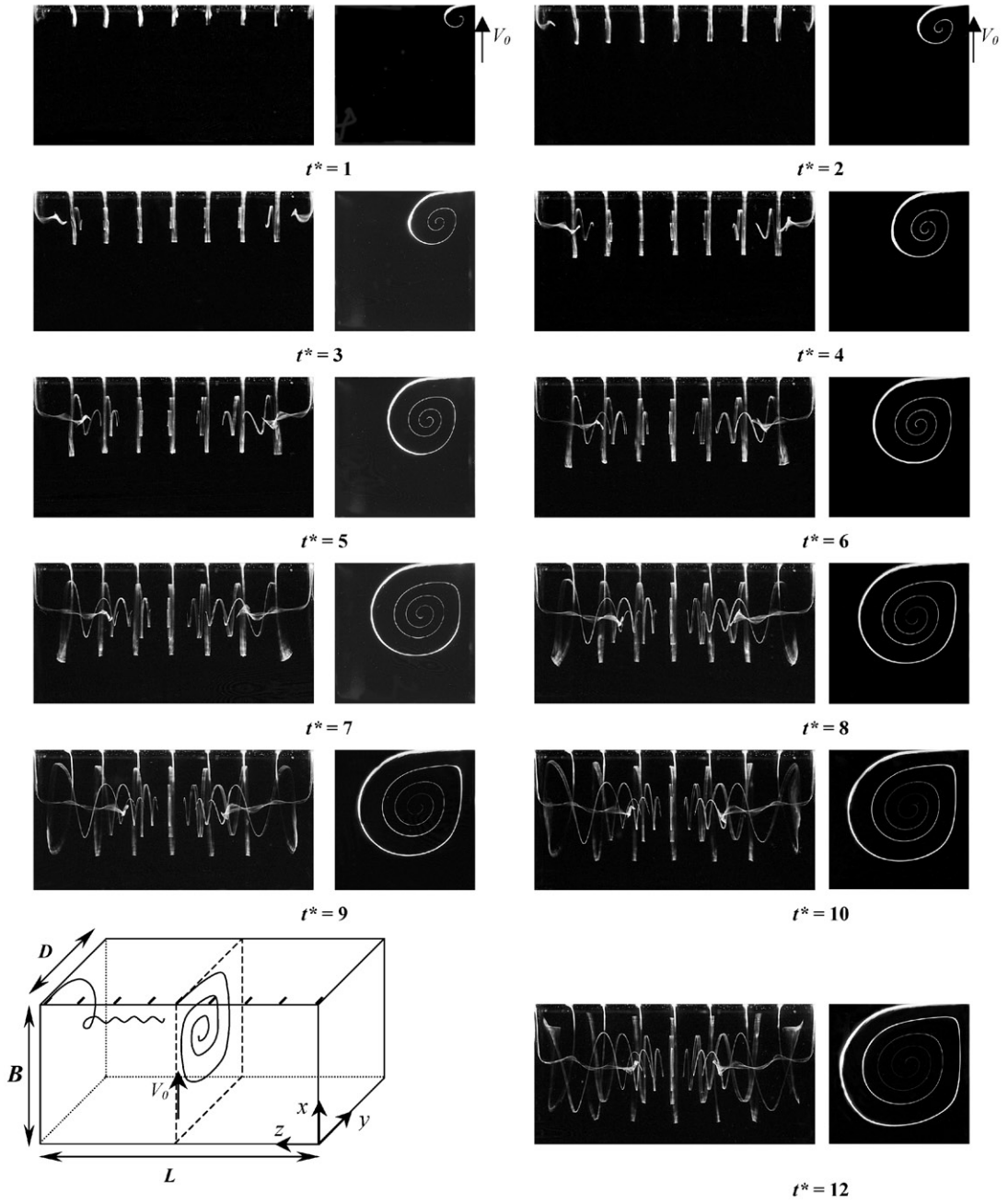

Fig. 5. Time-evolution of the dye-filament propagation inside the square cavity. Spanwise view and associated symmetry cross-plane.

cone-shaped structure. Thus, in sections $Z = 0.25$, 0.5 and 0.75, and their symmetrical ones, the flow loses clearly its 2-D character, respectively, from times $t^* = 3$, 4 and 5 for both cavities. So, the moment from which a given cross-plane becomes 3-D is independent of the cavity shape. From $t^* = 6$, the flow over the whole span of both cavities is fully affected by the 3-D spanwise currents, i.e., by the end-conditions. However, it is very important to note that the filament in the symmetry plane ($Z = 1$) keeps a 2-D form up to the final time $t^* = 12$ (no spanwise development is observed), indicating that the flow is symmetric with respect to this plane as it can be clearly seen in Figs. 5 and 6. However, from $t^* = 6$, and only from this time, the flow in the symmetry plane is different from the purely 2-D one; spanwise shear

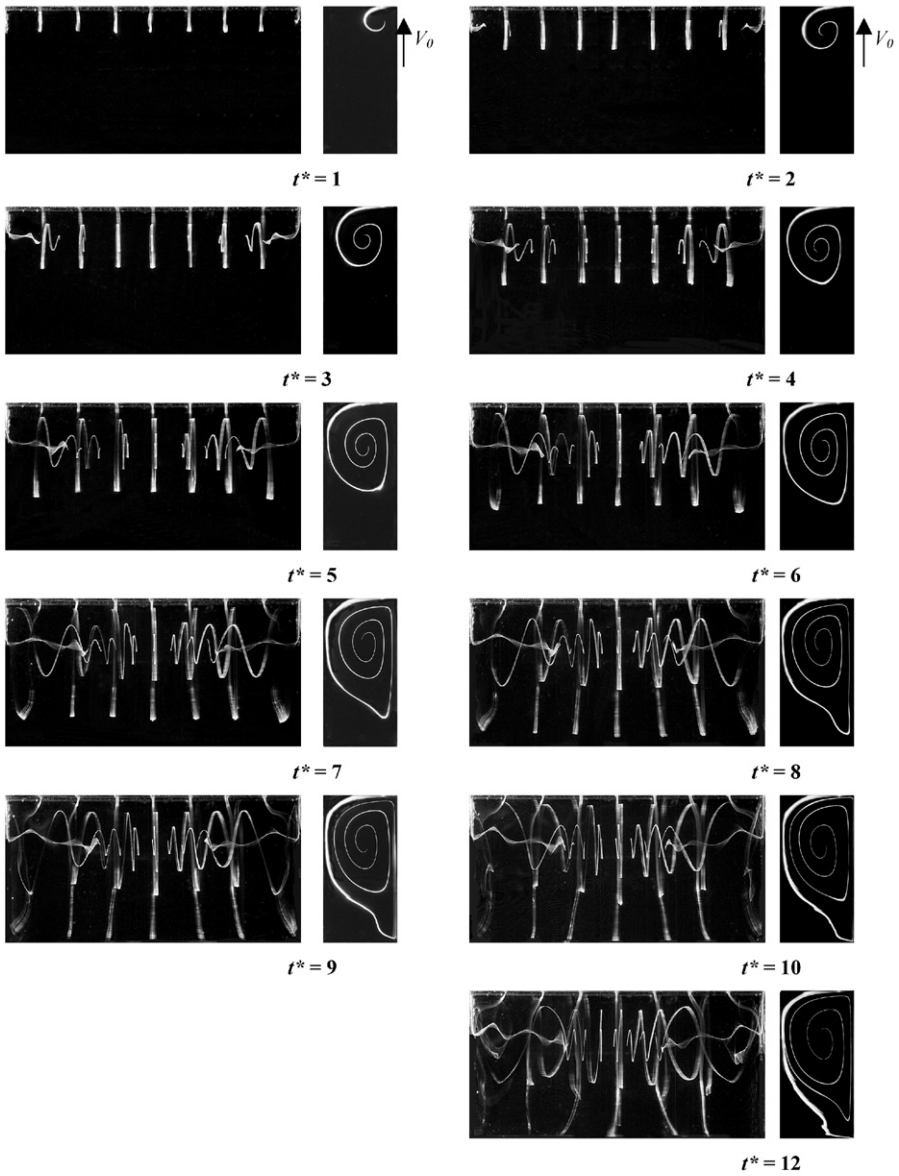

Fig. 6. Time-evolution of the dye-filament propagation inside the rectangular cavity. Spanwise view and associated symmetry cross-plane.

effects are no longer negligible (see Migeon, 2000). This spanwise current development is similar to that observed in the case of cylinder wakes by Polidori et al. (1992), Champion et al. (1992) and Pineau (1992).

Also notable (Figs. 5 and 6) is the peripheral outward current that moves the fluid towards the end-walls. This current is active in the periphery of the primary eddy. Spanwise outward currents existing in secondary eddies are not visible in Figs. 5 and 6 based on the electrochemical technique because the dye is only convected inside the primary eddy. However, these currents are well visible by using the particle-streak technique as presented in Section 4.

3.2. Quantitative examination

In order to give quantitative information on the propagation of the 3-D perturbation, time-evolutions of the ΔZ displacement of the filament extremities is given in Fig. 7. On the corresponding curves, the critical times, above mentioned, from which the flow in a cross-plane becomes 3-D (i.e., when ΔZ differs from zero) is clearly put on the fore.

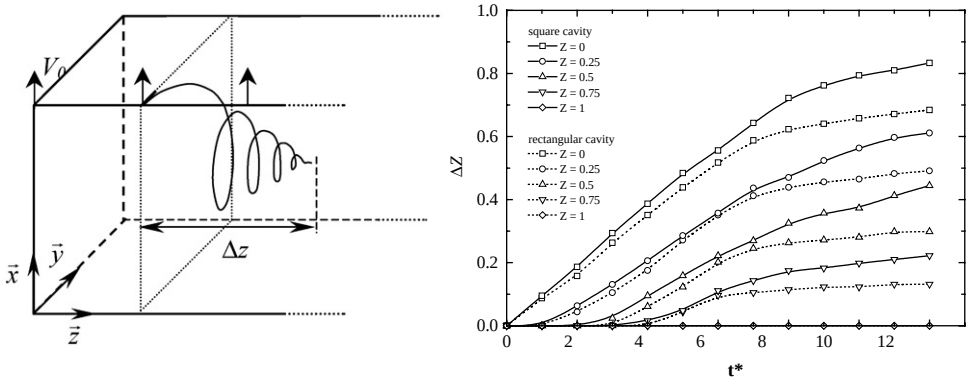

Fig. 7. Time-evolution of the ΔZ spanwise-displacement of the dye-filament for the square and rectangular cavities.

During a first phase of the flow establishment, i.e., up to $t^* = 6$, ΔZ-curves exhibit a quasi-linear part testifying that the 3-D perturbations propagate at a uniform velocity. Along this linear part, the 3-D perturbations propagate similarly in both cavities. The fact that the slope of the curves decreases when the axial coordinate Z increases indicates that the V_z velocity decreases when the distance from the wall increases. Along the linear part of the $Z = 0$-curve, the speed of filament progression is about $0.1V_0$.

For $t^* > 6$, the speeds of progression are slowed down by the opposition, in the symmetry plane, of the two currents coming from both half span-parts of the cavity. That is to say, once the two inward spanwise currents oppose, the third component (V_z) of the velocity vector is weakened in both cavities. Also, one can observe that at this time the velocity of the filament progression differs from a cavity to another: the 3-D perturbations propagate at lower velocity in the rectangular cavity than in the square one.

In wake-flows, Pineau (1992), Ehrmann (1996), Coutanceau et al. (2000) noted similar evolution of the spanwise currents. For example, for a 5:1 circular-cylinder wake-flow at $\mathrm{Re} = 1000$ the velocity of filament propagation is roughly similar to the one observe in the present experiment, i.e., about $0.1V_0$ (V_0 being the incident velocity). For a 5:1 semicircular-shell wake-flow at Re =600, the velocity of propagation is greater and equals to $0.3V_0$.

4. Particle-streak visualizations: corner and TGL vortices development

4.1. General information

The dye-emission technique materializes the dynamics of the global three-dimensionality of the flow, but does not provide information neither about the evolution of the end-wall eddies (i.e., the corner vortices), nor about the development of the secondary 3-D structures (Taylor–Gortler/Taylor vortices) distributed along the cavity span. The particle-streak technique applied in various horizontal and vertical span planes (see Section 2) allows to fill this gap. As examples, various flow pictures with their corresponding streamline-fields are proposed in Figs. 8 and 9. They show the temporal and spatial development of the flow in vertical span-planes, respectively, for the square and the rectangular cavities. To provide readers with a clearer image of the location of the spanwise structures with respect to the cross-plane ones, a "3-D view" of the flow is given at the top of each set of pictures. These sequences of visualizations appeared to be of primary importance for comparisons with numerical simulations. Indeed, they provide clues on the flow structure over the whole span including the precise location of the separating streamlines. In the figures, black arrows denote the flow orientation and direction (sense). As previously noted in Section 3, the flow preserves its symmetry with respect to the mid-cross plane at least up to $t^* = 12$.

The inward/outward currents prevailing in the primary eddy and the outward current occurring in secondary eddies can be clearly deduced from the pictures. It is noteworthy that, till $t^* = 12$, only the downstream secondary eddy develops inside the square cavity whereas both downstream and upstream secondary eddies develop in the rectangular cavity (Migeon et al., 2000).

For briefness, pictures of the horizontal span-planes are not reported in this paper. However, the whole of both horizontal and vertical visualized span-planes have been analyzed in order to obtain the "3-D schematics" of the corner and TL vortices, respectively, given in Figs. 10, 11, 13 and 14.

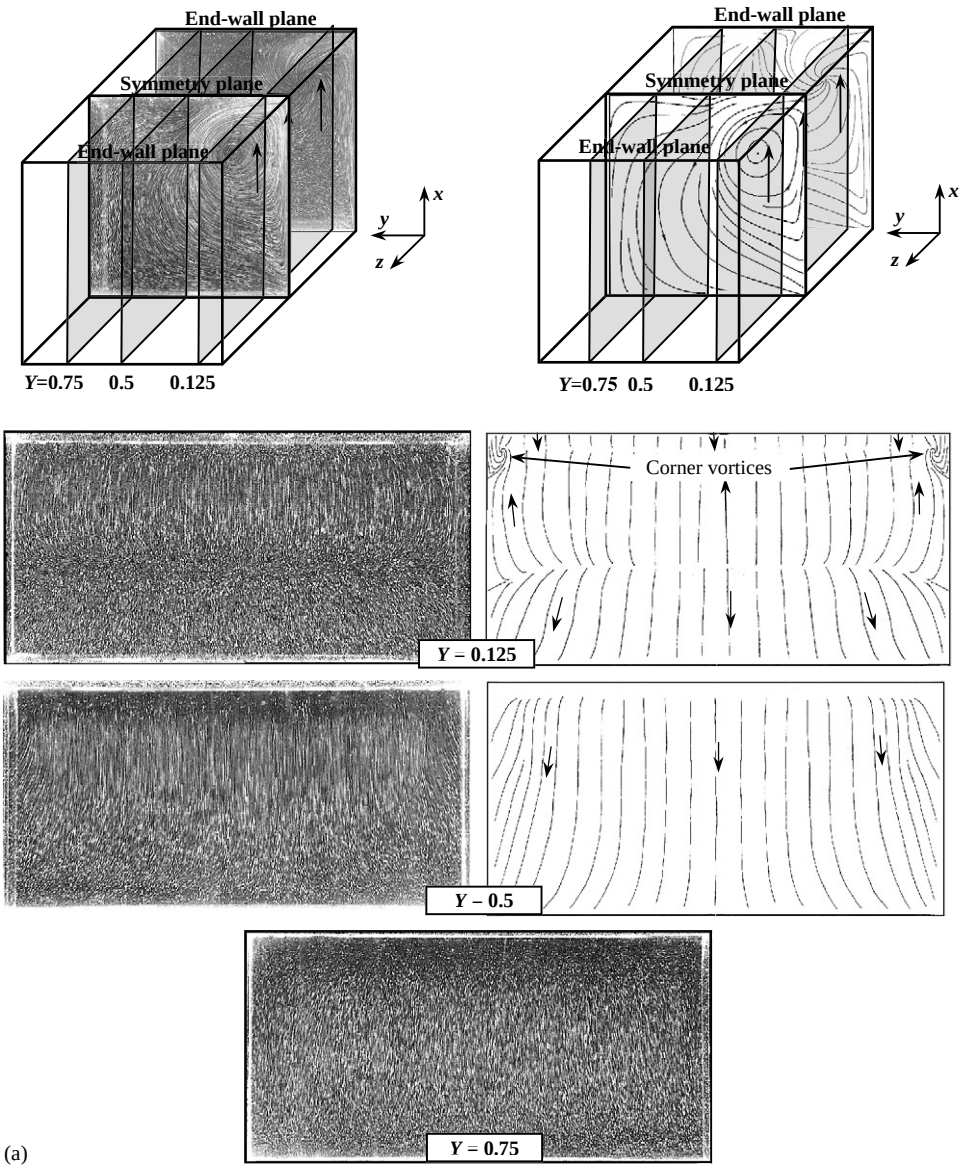

Fig. 8. Flow visualizations and associated streamline fields in various vertical span planes of the square cavity at (a) $t^* = 4$, (b) $t^* = 6$, (c) $t^* = 8$ and (d) $t^* = 12$.

4.2. End-wall corner vortices

In this subsection, the formation and development of the corner vortices are described. A detailed numerical analysis of the role of these vortices has recently been proposed by Chiang et al. (1997) for the case of the flow inside a 3:1 square cavity at Re =1500. These authors distinguished "x-plane" and "y-plane" corner vortices the occurrence of which was found to be rather "dependent on the spanwise and the primary circulating flow-motions". These vortices aid the fluid coming from the outward currents to engulf into the primary core, i.e., into the inward current, acting as "a suction pump near the end wall". In fact, Chiang et al. were not the first to mention the presence of corner vortices; however, they seem to be the first to clearly depict their role. In spite of general agreements with their conceptual view, the present results exhibit unknown phenomena and shed some new light on the temporal and spatial development of these end-wall corner-vortices.

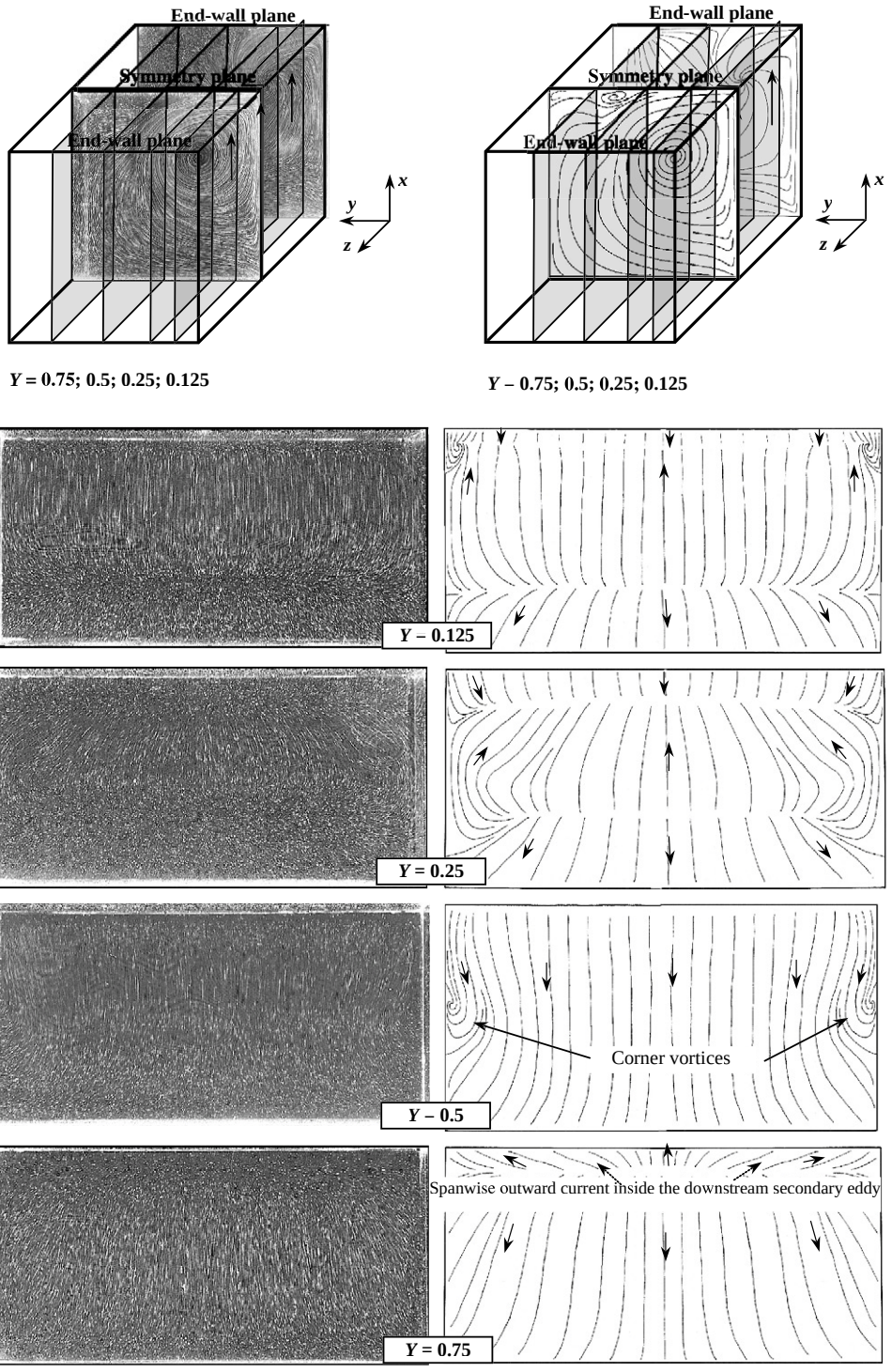

(b)

Fig. 8 (*continued*).

Indeed, as it is shown in Figs. 10 and 11, respectively, for the square and the rectangular cavities, the present experimental analysis reveals that a unique quasi-toroidal corner vortex develops at the two end-walls. This vortex surrounds the primary eddy core, with its axis following the primary eddy streamlines. Therefore, at $t^* = 2$, the

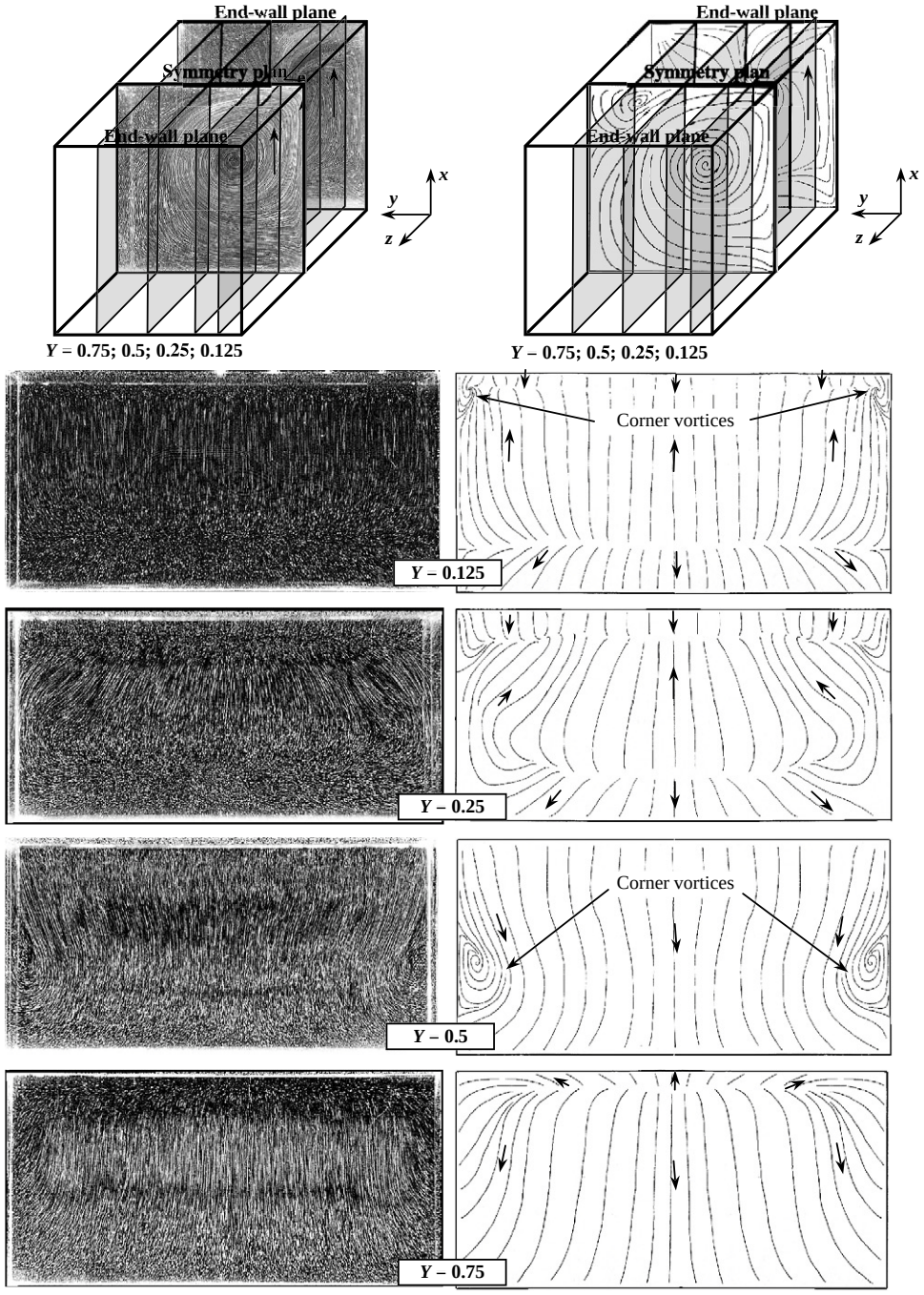

(c)

Fig. 8 (*continued*).

end-wall corner vortex is similar in both cavities and it is located in the "upper right quarter-part" of the cavity. With time increasing, it penetrates inside the cavity following the primary eddy progression. From $t^* = 4$, the cavity walls (and consequently the cavity shape) begin to interact: in the rectangular cavity, the end-wall vortex elongates similarly to the primary eddy, whereas, in the square cavity, it keeps a roughly circular shape. Consequently, at the final time-stage $t^* = 12$, the corner vortex is in its "left and upstream parts" far less extended in the rectangular cavity than in the square one. In both cavities, the corner-vortex size decreases in the primary eddy flow direction.

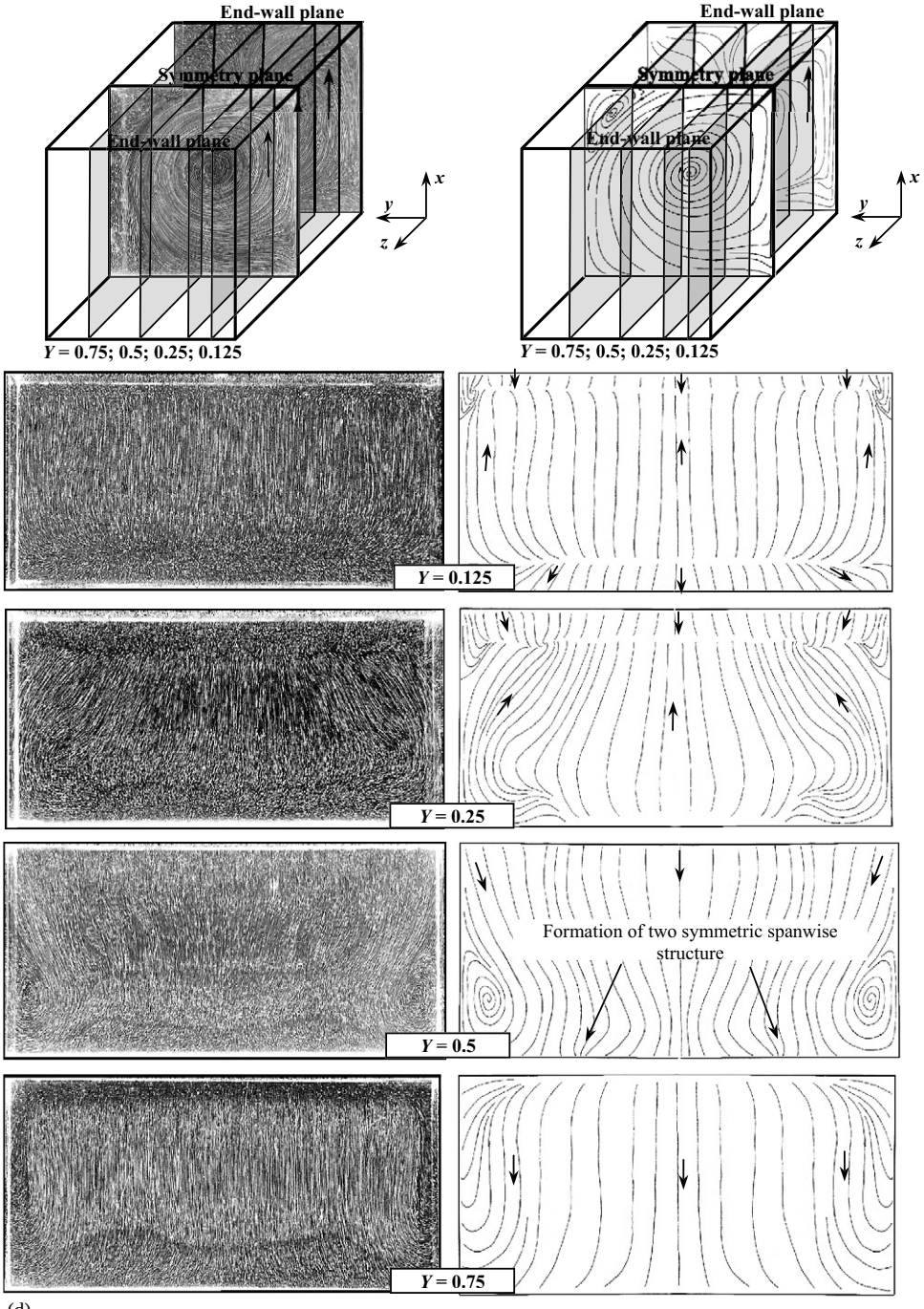

(d)

Fig. 8 (*continued*).

However, since the end-wall vortex surrounds the primary eddy, one can wonder why its rotating movement is not observed in each visualized vertical plane (Figs. 8 and 9)? As it was previously noticed, the corner vortex possesses a toroidal-type shape. Therefore, the more favorable planes for the observation of its rotating motion are planes perpendicular to its axis. In such a way, at $t^* = 12$, i.e., when the corner vortex is almost fully developed, the mid-horizontal and -vertical planes ($Y = X = 0.5$ for the square cavity and $2Y = X = 0.5$ for the rectangular one) are the

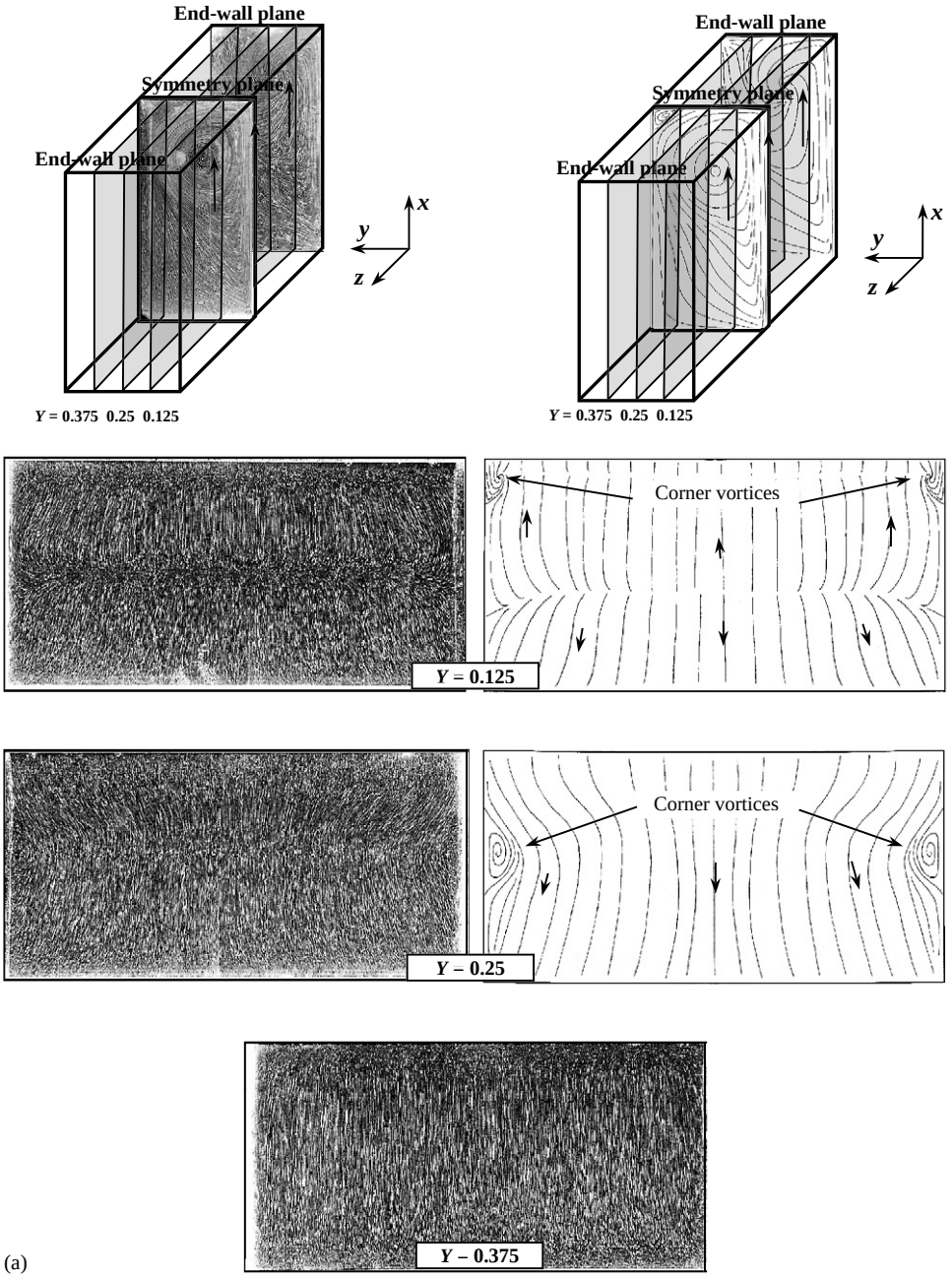

Fig. 9. Flow visualizations and associated streamline fields in various vertical span planes of the rectangular cavity at (a) $t^* = 4$, (b) $t^* = 6$, (c) $t^* = 8$ and (d) $t^* = 12$.

most favorable ones to observe corner vortex rotation (Figs. 8 and 9). In the other planes examined, the rotating movement cannot be observed because the corner vortex is cut on its periphery (see the typical movement of the streamlines near the end-walls).

Although the existence of the corner vortex has been reported for a long time, its precise origin is not clearly understood yet. Our study reveals that the origin of such a vortex is centrifugal (as described below) and similar to that of the vortex which develops at the end-walls of others typical circular flows limited in span by stationary end-walls (Taylor–Couette flow between rotating cylinders, Gortler flow over curved surface, etc.); the latter case has been finely

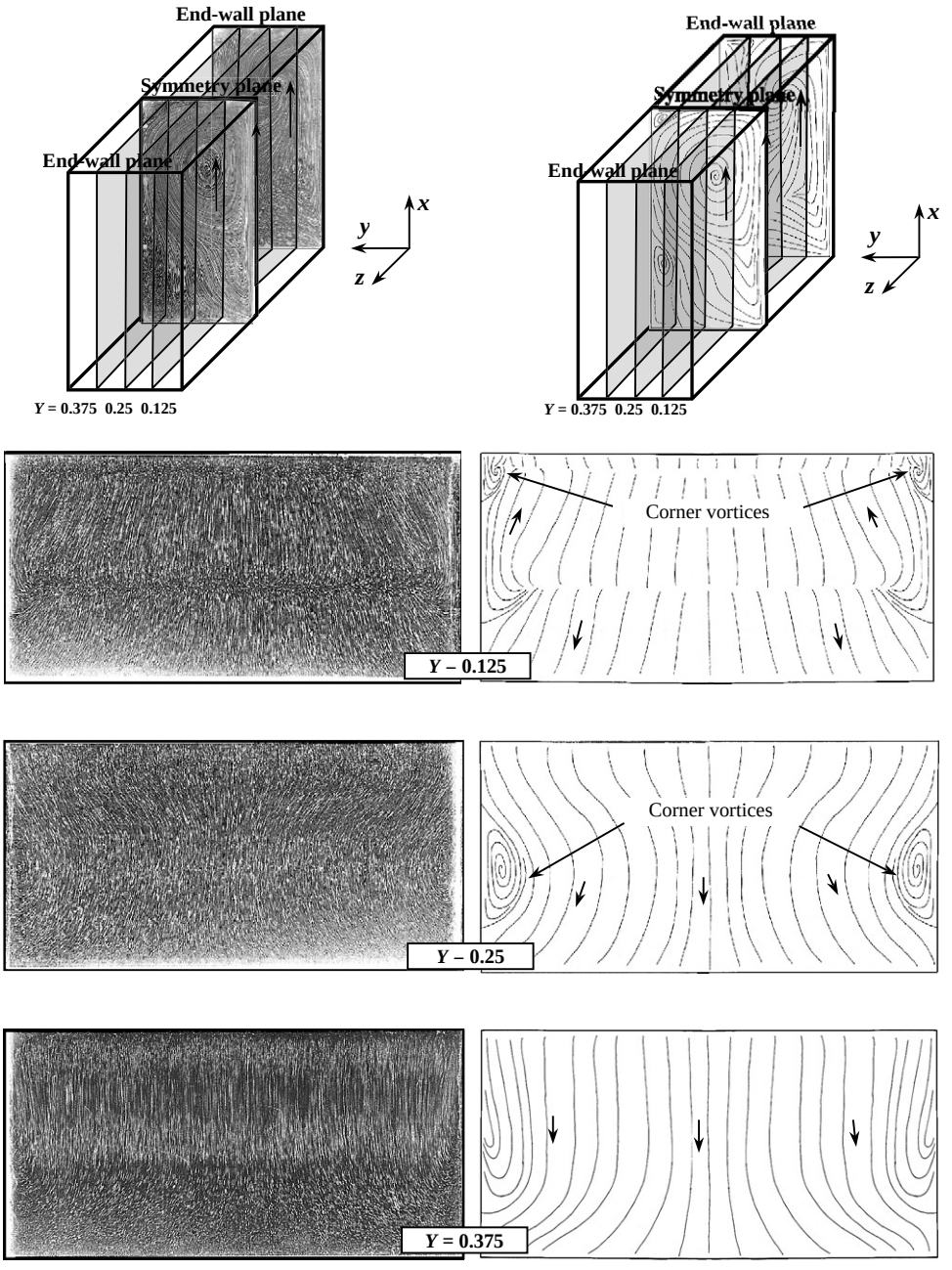

(b)

Fig. 9 (*continued*).

examined by Petitjeans (1992) and Petitjeans et al. (1995). It is also similar to those mentioned by Coutanceau et al. (2000) in the case of limited-in-span recirculating wake flows.

In Fig. 12, a schematic-comparison of the spanwise flow evolution in a square lid-driven cavity with and without 3-D effects is presented. We denote $\boldsymbol{r}$ and $\boldsymbol{\theta}$, respectively, the radial and the azimuthal axis associated with the circular motion of the primary eddy and $\boldsymbol{V_r}$ and $\boldsymbol{V_\theta}$ the velocity components measured along the $\boldsymbol{r}$ and $\boldsymbol{\theta}$ axes.

In a 2-D configuration, the flow structure is invariant over the whole span of the cavity (infinite SAR hypothesis), the streamlines are closed. There exists a balance between the centrifugal and the radial pressure forces exerting on a fluid particle (Fig. 12); the former is pointed outward and the latter inward.

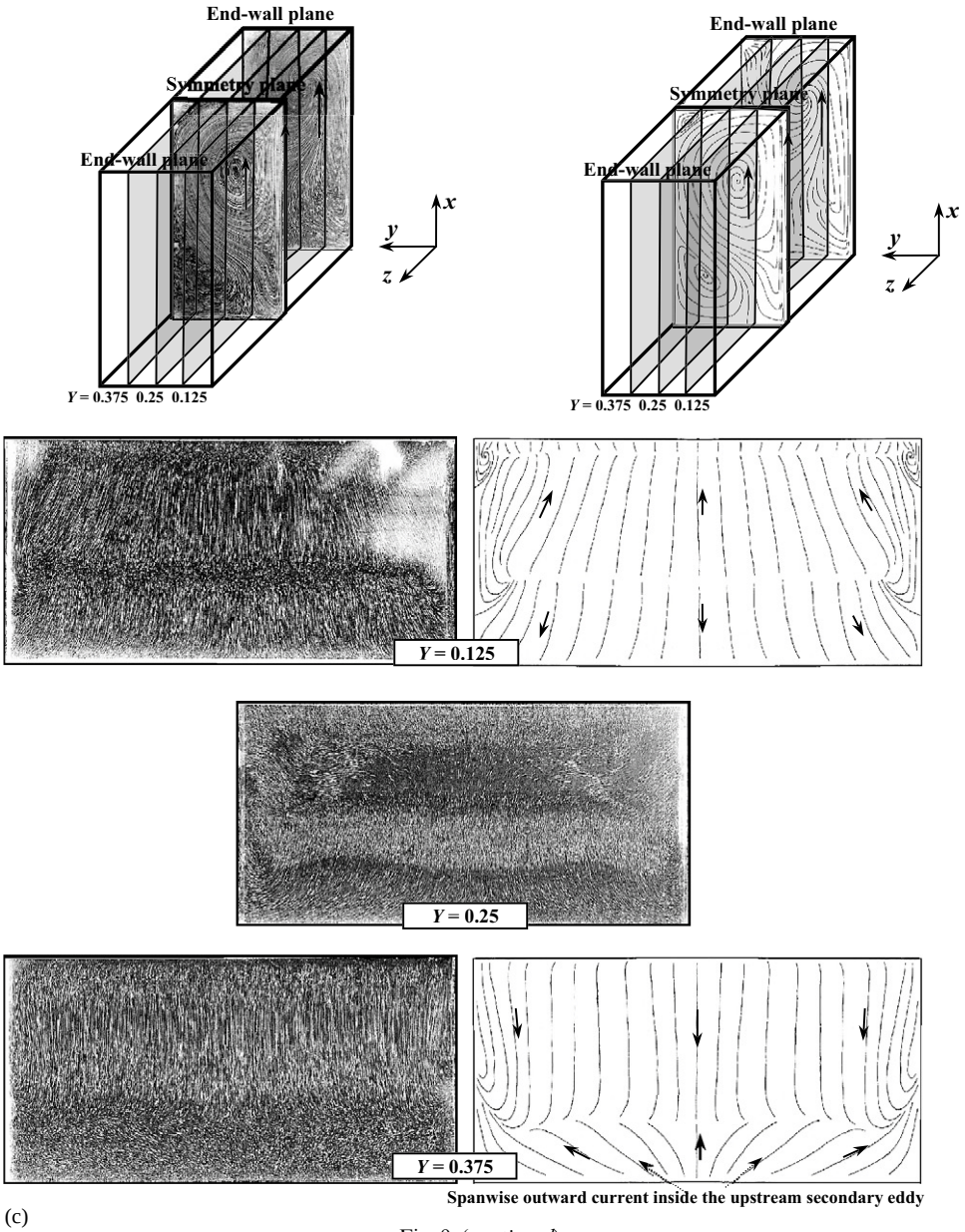

(c)

Fig. 9 (*continued*).

In a cavity of finite length, due to end-conditions, a transverse gradient tamper the azimuthal velocity $\boldsymbol{V_\theta}$ inducing the formation of a boundary layer (see black bold arrows on Fig. 12b). The centrifugal force $F_c = V_\theta^2/r$, being dependent on the velocity magnitude, increases with the end-wall distance until the velocity becomes nearly constant outside the boundary layer. This variation of the centrifugal force creates an unbalance between the centrifugal (F_c) and the radial pressure (F_p) forces. Therefore, in the boundary layer, the centrifugal force being insufficient to counterbalance the radial pressure one, i.e., to conduct the rotating movement of the primary eddy streamlines, the latter are attracted towards the primary eddy core as it is represented in Fig. 12b and as visualized in the end-wall plane ($Z = 0$; see Figs. 8 and 9); the core of the primary eddy becomes an inward spirally point. Then, an opposition exists between the sense of the radial velocity V_r of the fluid confined inside the boundary layer and the one located outside; outside the boundary layer, the flow is pointed outward whereas inside the boundary layer, due to force unbalance, it is pointed inward. By continuity this unbalance creates the so-called corner vortex at both end-walls.

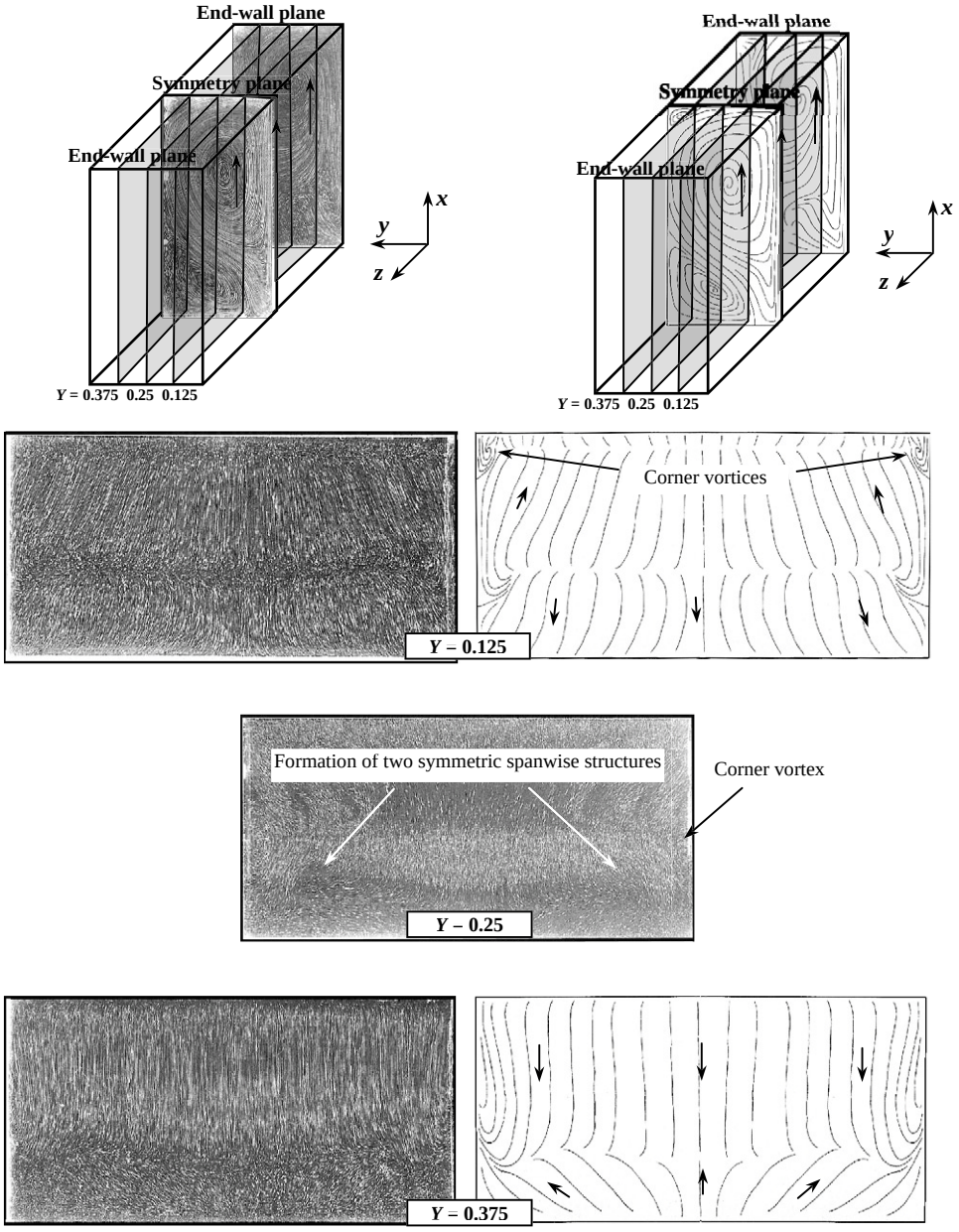

(d)

Fig. 9 (*continued*).

Therefore, in order to appraise whether or not the corner vortices will form, the region where the radial velocity V_r is positive, outside the two end-wall boundary layers, has to be detected. Considering this expectation, in the region "above" the primary eddy core, the V_r velocity being negative outside the boundary layer (flow directed inward), so the corner vortex does not form in this region (Figs. 10 and 11).

However, it is important to mention, that even if corner vortices are centrifugal induced, they are not to be confused with the TGL or TL vortices which are also centrifugal induced but arise from the flow instability itself (such as the Gortler vortices in curved conduits (Petitjeans, 1992; Petitjeans et al., 1995) or Taylor–Couette ones in the gap between rotating cylinders).

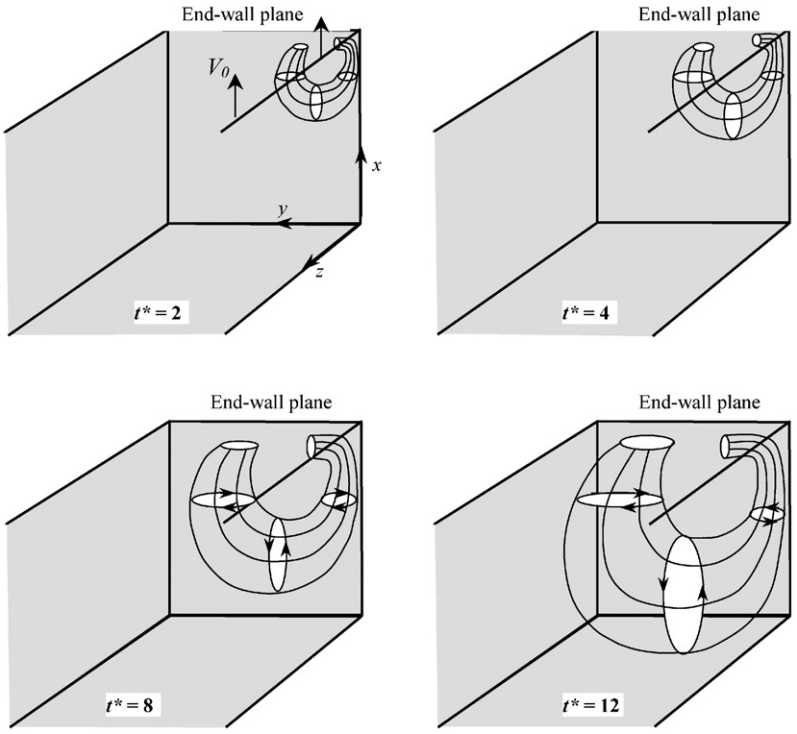

Fig. 10. Corner vortex schematization in the square cavity for times $t^* = 2$, 4, 8 and 12.

4.3. Taylor-like vortices

Flow instability induces counter-rotating vortex pairs (secondary 3-D structures) which constitute the third main manifestation of the flow three-dimensionality. As previously stated, the experimental Stanford's group put forward the development of counter-rotating vortices as soon as Re =1000 both during the establishment phase and the fully developed one. In the present experiments, as it can be verified in Figs. 8 and 9, for Re =1000, no pairs of counter-rotating vortices develop until the final time of visualization $t^* = 12$; only the formation of an "emergent" structure is observed. This one characterizes the initial development of the counter-rotating pairs and constitutes the second manifestation of the flow TL instability (the first manifestation is described below). This structure is characterized by the convergence of the streamlines in the way put forward on the streamline fields of Figs. 8 and 9 and Figs. 13 and 14. This structure appears at $t^* = 10$ in both cavities and close to the spanwise location $Z = 0.5$ and 0.29 (and the symmetric ones), respectively, for the square and the rectangular cavities. This phenomenon points out that the flow instability first manifests just near the corner vortices and in a similar way here and there the symmetry plane $Z = 1$.

Furthermore, one can note that the instability manifests only at the foot of the vertical plane, i.e., in the "upstream part" of the primary eddy, as it is schematized in Figs. 13 and 14. So, during the establishment phase, the Taylor-type vortices (or their initial structure) only develop in a very localized zone and not all around the primary eddy as it was previously stated (Koseff and Street, 1984). Therefore, in both cavities, the upstream part of the primary eddy seems to be the most unstable part of the flow.

It has to be mentioned that similar converging-streamline structures have been observed by Coutanceau et al. (2000) in the span-section of the wake of a semicircular shell for Reynolds numbers greater or equal to 200. These authors showed that, with increasing time and Reynolds number, these structures evolve into well-formed counter-rotating vortices. The study of cavity flows for Reynolds numbers greater than 1000 will also show the same phenomenon; this work is presently in progress.

As mentioned above, the formation of the converging-streamline structures only constitutes the second stage of flow instability development. The first stage does not generate a particular structure but produces a modification on the mixing process. In order to appreciate such a phenomenon, visualizations were performed by using the particle-streak technique in a special form. After seeding particles in the cavity area, a large waiting period generates in the

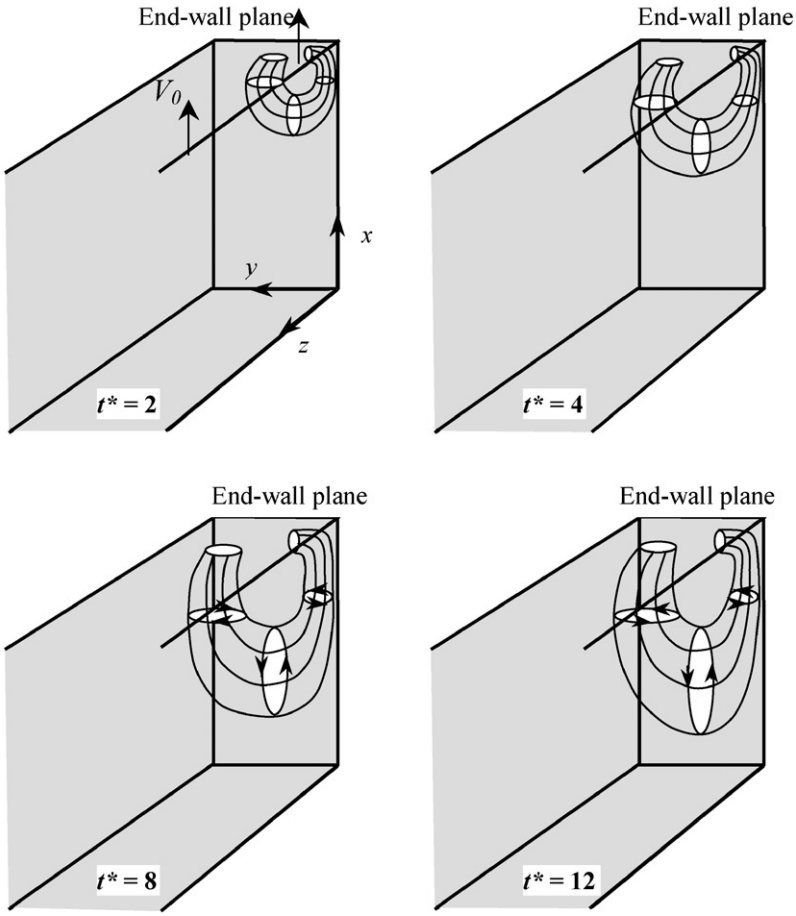

Fig. 11. Corner vortex schematization in the rectangular cavity for times $t^* = 2$, 4, 8 and 12.

downstream (upper) part of the cavity a zone without particles due to sedimentation effects. During flow development, the zone without particles is convected inside the cavity area (Fig. 15). In cross-section (Fig. 15b), the separation line between the zones with and without particles identifies the delimiting line of the mixing-zone area similarly to the dye lines issued from the dye-emission technique. Therefore, if the mixing zone propagated in a similar manner over the whole span of the cavity, on the spanwise views of Fig. 15a the separated line would be straight. One can note that it is not the case. Instead, an oscillation phenomenon is observed. This oscillation corresponds to a reduction of the propagation of the mixing-zone area. This is the first manifestation of the flow instability which acts from $t^* = 7$ in the present observations.

5. Conclusion

In the framework of a study on the benchmark lid-driven cavity flow, the manner in which three-dimensionalities set up and develop with time from rest has been examined at a Reynolds number of 1000. This approach permits the flow patterns to be visualized and followed with time from their initial onset to a final time of observation $t^* = 12$ in steps $\Delta t^* = 1$.

This experimental study demonstrates the ability of the start-up flow analysis, combined with the dye-emission and the particle-streak techniques, to give insights into the 3-D flow behavior. Those results complete the information previously given on the quasi-2-D flow structure which develops inside the symmetry plane ($Z = 1$) of variously shaped lid-driven cavities (Migeon et al., 1998; Migeon et al. 2000).

From this analysis, new physical characteristics have been put in evidence.

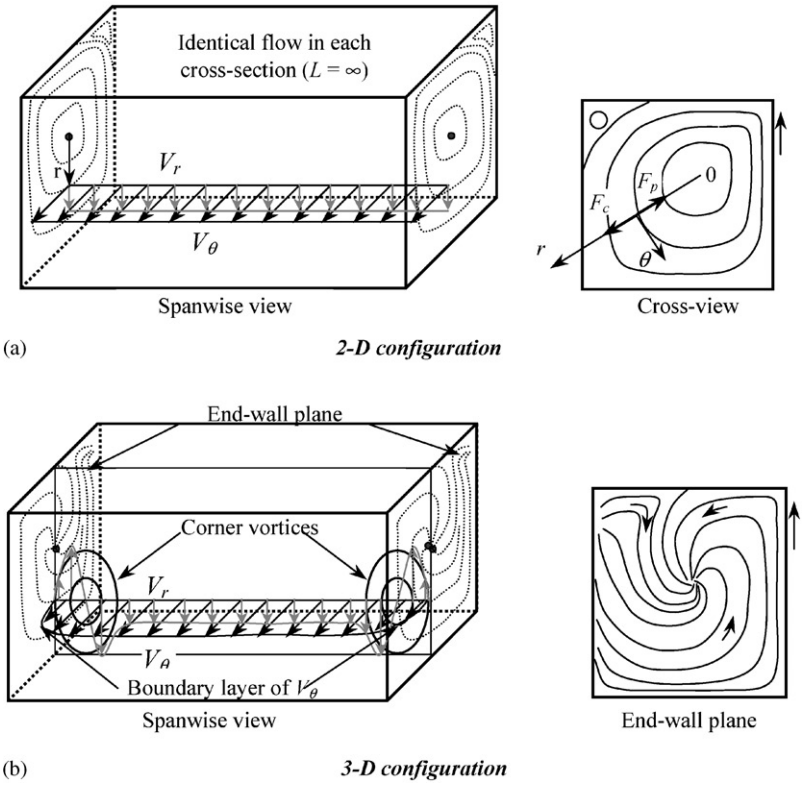

Fig. 12. Spanwise evolution of the V_r and V_θ velocity components for the 2-D and 3-D square cavity. Principle of the corner vortices development.

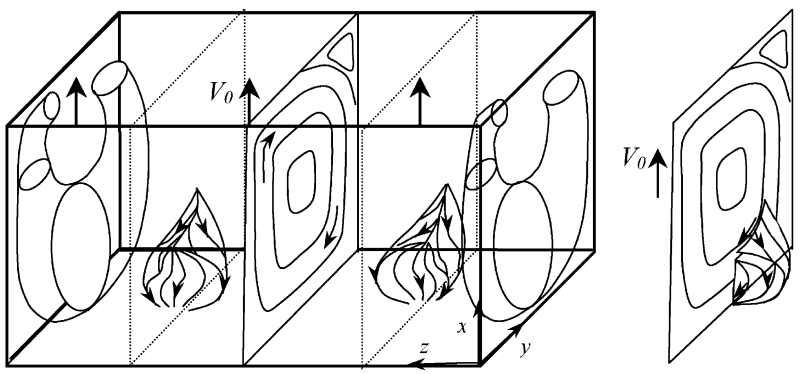

Fig. 13. Schematization and location of the two symmetric spanwise structures representing the initial development of Taylor-type vortices in the square cavity at time $t^* = 12$.

(i) Initially the flow can be assimilated to the 2-D flow. With increasing time, due to the no-slip conditions prevailing on both end-walls, spanwise currents develop symmetrically towards the symmetry plane and successively affect each cross-section which become 3-D. It has been shown that the time from which a given cross-section starts to become clearly 3-D is identical in the square and rectangular cavities. From $t^* = 6$, the flow over the whole span of the two cavities is influenced by the end-wall conditions. However, it was clearly shown that the symmetry plane flow keeps a quasi-2-D configuration (but not purely 2-D) all over the investigated time-range. The ''meeting'' of

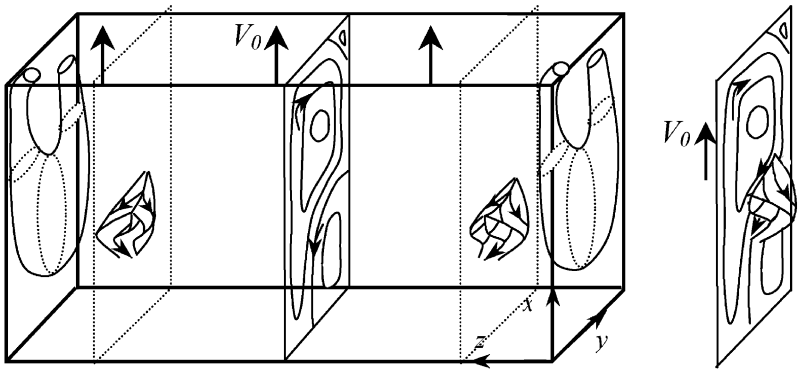

Fig. 14. Schematization and location of the two symmetric spanwise structures representing the initial development of Taylor-type vortices in the rectangular cavity at time $t^* = 12$.

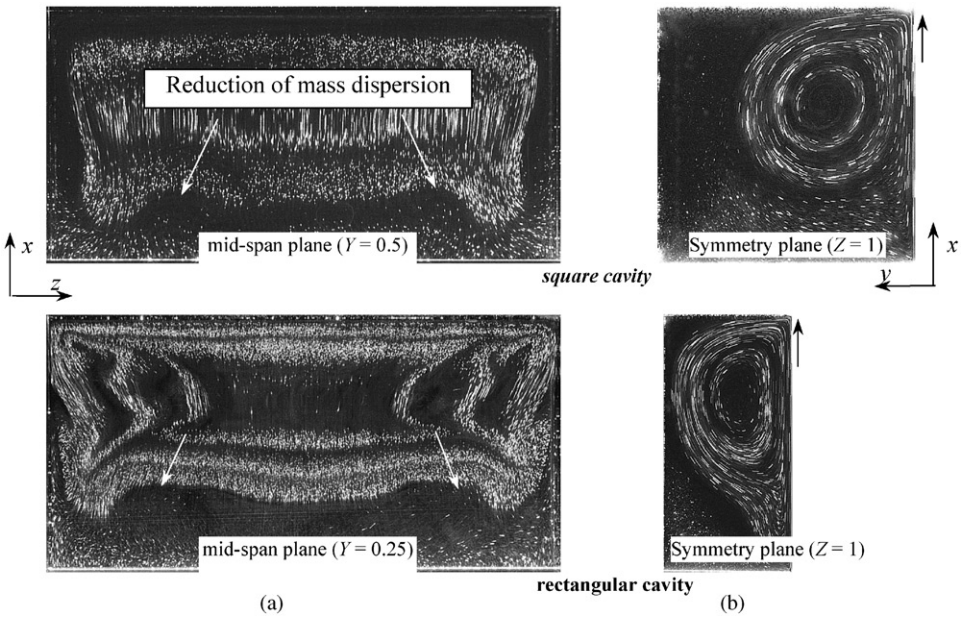

Fig. 15. Span and cross-flow visualizations performed with a specific particle-streak technique in the square and the rectangular cavities at $t^* = 8$.

the two opposed spanwise currents in the symmetry plane induces a clear reduction of the V_z-velocity magnitude, and that, in a different way in the square and the rectangular cavities.

(ii) Concerning the end-wall corner vortices, a new conceptual view of their structure is proposed. Indeed, for the first time, it is put forward that there exists a unique corner vortex at the two end-walls as opposed to what was claimed so far. This vortex is quasi-toroidal and has a centrifugal origin; it greatly depends on the cavity shape (essentially beyond $t^* = 4$, i.e., when the structure of the primary eddy is itself influenced by the cavity shape). The similarity of the present end-wall vortex with similar vortex which develops at the end-walls of others centrifugal flows, such as the Taylor–Couette and the Gortler ones and even the recirculating flows of bluff body wakes limited by end-plates, was proposed.

(iii) Concerning the TL instability development, it is shown that during the establishment phase of the flow, at Re =1000, no counter-rotating vortices develop in both cavities. However, for the first time, according to the author's knowledge, the two initial phases of this instability manifestation have been put in evidence, respectively, at $t^* = 7$ and 10 in both cavities. The first phase corresponds to a mixing-process reduction and the second one to

the formation of emergent structures characterized by the convergence of streamlines in span-planes. Also, it has been put in evidence that the instability only manifests in a very localized zone, i.e., the upstream part of the primary eddy which is then considered as the most unstable part of the flow. The Taylor-type structure only appears right near the two corner vortices thus clearly indicating that perturbations induced by the presence of these corners vortices are responsible for instability manifestation.

The study of the start-up cavity flow for Reynolds numbers larger than 1000 is presently in progress and will be part of a future paper (Migeon, 2002).

References

Aidun, C., Triantafillopoulos, N., Benson, J., 1991. Global stability of a lid-driven cavity with throughflow: flow visualization studies. Physics of Fluids A3, 2081–2091.

Badr, H., Coutanceau, M., Dennis, S., Menard, C., 1990. Unsteady flow past a rotating circular cylinder at Reynolds numbers 10^3 and 10^4. Journal of Fluid Mechanics 220, 459–484.

Champion, J.-L., Coutanceau, M., 1992. Development of the near wake structure on a cantilevered circular cylinder with free-end. In: Eckelmann, H., Graham, J.M.R., Huerre, P., Monkewitz, P.A. (Eds.), Bluff-Body Wakes, Dynamics and Instabilities (IUTAM Symposium Göttingen). Springer, Berlin, pp. 43–46.

Chiang, T.P., Sheu, W.H., 1997. Numerical prediction of eddy structure in a shear-driven cavity. Computational Mechanics 20, 379–396.

Chiang, T.P., Hwang, R.R., Sheu, W.H., 1997. On end-wall corner vortices in a lid-driven cavity. Journal of Fluids Engineering 119, 201–204.

Chiang, T.P., Sheu, W.H., Hwang, R.R., 1998. Effects of the Reynolds number on the eddy structure in a lid-driven cavity. International Journal for Numerical Methods in Fluids 26, 557–579.

Coutanceau, M., Pineau G., 1997. Some typical mechanisms in the early phase of the vortex-shedding process from particle-streak visualization. In: The Visualization Society of Japan (Ed.), Atlas of Visualization III. CRC Press, Boca Raton, pp. 43–68.

Coutanceau, M., Migeon, C., Pineau, G., Texier A., 1996. Starting flow inside a rectangular-section cavity as function of Reynolds number. In: Wei, Q.D. (Ed.), Proceedings of the Fourth Asian Symposium on Visualization, International Academic Publishers, pp. 65–68.

Coutanceau, M., Migeon, C., Erhmann, P., 2000. Particulars of the cross- and spanwise near-wake development of a short semicircular-section shell, through the transition Re-range ($60 \leqslant Re \leqslant 600$). Journal of Visualization 3 (1), 9–26.

De Dahl Davis, Mallinson, G., 1976. An evaluation of upwind and central difference approximations by a study of recirculating flow. Computer and Fluids 4, 29–43.

Deville, M., Morchoisne, Y., 1992. Numerical simulation of 3-D incompressible unsteady viscous laminar flows. International Workshop, Paris, France.

Ehrmann, P., 1996. Etude comparative de la formation des sillages en fonction de la forme des obstacles: application à la coque semi-circulaire. Thèse de Doctorat de l'Université de Poitiers, France.

Freitas, C.J., Street, R.L., 1988. Non-linear transient phenomena in a complex recirculating flow: a numerical investigation. International Journal for Numerical Methods in Fluids 8, 669–801.

Freitas, C.J., Street, R.L., Findikakis, A.N., Koseff, J.R., 1985. Numerical simulation of three-dimensional flow in a cavity. International Journal for Numerical Methods in Fluids 5, 561–575.

Gaskell, P., Summers, J., Thompson, H., 1996. Creeping flow analyses of free surface cavity flows. Theoretical and Computational Fluid Dynamics 8, 415–433.

Ghia, U., Ghia, K.N., Shin, C.T., 1982. High-Re solutions for incompressible flow using the Navier–Stokes equations and a Multigrid method. Journal of Computational Physics 48, 387–411.

Guermond, J-L., Migeon, C., Pineau, G., Quatarpelle, L., 2002. Start-up flows in a 3D rectangular driven cavity of aspect ratio 1:1:2 at $Re = 1000$. Journal of Fluid Mechanics 450, 169–199.

Koseff, J.R., Street, R.L., 1982. Visualization studies of a shear driven three-dimensional recirculating flow. In: Proceedings Thermophysics and Heat transfer Conference on Three-Dimensional Turbulent Shear Flows. AIAA/ASME, St. Louis, pp. 23–31.

Koseff, J.R., Street, R.L., 1984a. Visualization studies of a shear driven three-dimensional recirculating flow. Journal of Fluids Engineering 106, 21–29.

Koseff, J.R., Street, R.L., 1984b. On end wall effects in a lid-driven cavity flow. Journal of Fluids Engineering 106, 385–389.

Koseff, J.R., Street, R.L., 1984c. The lid-driven cavity flow: a synthesis of qualitative and quantitative observations. Journal of Fluids Engineering 106, 390–398.

Liou, T., Liao, C., 1997. Study of pulsative flows in lateral aneurysm model on a straight parent vessel using particle tracking velocimetry. The First Pacific Symposium on Flow Visualization and Image Processing, Honnolulu, pp. 639–644.

Migeon, C., 2000. Contribution à l'analyse de l'écoulement tridimensionnel instable s'établissant à l'intérieur de cavités cylindriques. Thèse de Doctorat de l'Université de Poitiers.

Migeon, C., 2002. Details on the start-up development of the Taylor–Gortler-Like vortices inside a square-section lid-driven cavity for $1000 \leqslant Re \leqslant 3200$. Experiments in Fluids 33, 594–602.

Migeon, C., Texier, A., Pineau, G., 1998. Start-up flow in various trapezoidal-section lid-driven cavities. Proceedings of the FEDSM'98, June 21–25, Washington, DC.

Migeon, C., Texier, A., Pineau, G., 2000. Effects of lid-driven cavity shape on the flow establishment phase. Journal of Fluids and Structures 14, 469–488.

Ohmi, O., Coutanceau, M., Daube, O., Loc, T.L., 1991. Further experiments on vortex formation around an oscillating and translating airfoil at large incidences. Journal of Fluid Mechanics 225, 607–630.

Petitjeans, P., 1992. Etude expérimentale des instabilités de couches limites sur des parois concaves : Instabilité de Görtler. Thèse de Doctorat de l'Université Paris VI, France.

Petitjeans, P., Wesfreid, J., Deplano, V., Vlad, G., 1995. Effect of curvature on the velocity profile and boundary layer in flow through a curved channel. La Recherche Aérospatiale 2, 125–138.

Pineau, G., 1992. Mise en évidence et évaluation des effets tridimensionnels dans l'écoulement instationnaire autour d'un cylindre circulaire d'envergure finie. Thèse de Doctorat de l'Université de Poitiers, France.

Pineau, G., Texier, A., Coutanceau, C., Ta Phuoc Loc, 1992. Experimental et numerical visualization of the 3D flow around a short circular cylinder fitted with endplates. In: Y. Tanida, H. Miyashiro (Eds.), Proceedings of the Sixth International Symposium on Flow Visualization. Springer, Berlin, pp. 343–347.

Polidori, G., 1994. Etude par visualisation de sillages tridimensionnels, application à un prifil d'aile rectangulaire. Thèse de Doctorat de l'Université de Poitiers, France.

Polidori, G., Pineau, G., Abed Meraïm, K., Coutanceau, M., 1992. Shedding process of the initial vortices from impulsively started cylinders at $\mathrm{Re} = 1000$; end and body geometry effects. In: Eckelmann, H., Graham, J.M.R., Huerre, P., Monkewitz, P.A. (Eds.), Bluff-Body Wakes, Dynamics and Instabilities (IUTAM Symposium Göttingen). Springer, Berlin, pp. 285–288.

Prasad, A., Perng, C., Koseff, J., 1988. Some observations on the influence of longitudinal vortices in a lid-driven cavity flow. First National Fluids Dynamics Congress, Cincinnati, OH, pp. 288–295.

Savvides, C., Gerrard, J., 1984. Numerical analysis of the flow through a corrugated tube with application to arterial prostheses. Journal of Fluid Mechanics 138, 129–160.

Shankar, P., Deshpande, M., 2000. Fluid mechanics in the driven cavity. Annual Review of Fluid Mechanics 32, 93–136.